J. Fluid Mech. (2000), *vol.* 421, *pp.* 15–38. Printed in the United Kingdom

New insight into the generation of ship bow waves

By E. FONTAINE[1]†, O. M. FALTINSEN[2] AND R. COINTE[3]

[1]Ocean Engineering Laboratory, UCSB, Santa Barbara, CA 93106-1080, USA

[2]Norwegian University of Science and Technology, N-7034 Trondheim, Norway

[3]Ecole Polytechnique, Département de Mécanique, 91128 Palaiseau, France

(Received 24 April 1998 and in revised form 26 November 1999)

The generation of ship bow waves is studied within the framework of potential flow theory. Assuming the ship bow to be slender, or thin, a pattern of the flow is derived using the method of matched asymptotic expansions. This method leads to the determination of three different zones in which three asymptotic expansions are performed and matched. To first order with respect to the slenderness parameter, the near-field flow appears to be two-dimensional in each transverse plane along the bow. However, it is demonstrated that three-dimensional effects are important in front of the ship and must be taken into account in the composite solution. This leads to a three-dimensional correction to be added to the two-dimensional solution along the ship. The asymptotic approach is then applied to explain the structure of the bow flow in connection with experimental observations and numerical simulations.

1. Introduction

Ship bow waves have received considerable attention, in particular because of their nonlinear character. Experimentally, it is observed that steep diverging waves generally originate in the bow region (see e.g. Miyata & Inui 1984; Dong, Katz & Huang 1997). From a theoretical point of view, Ogilvie (1967) extended the earliest high-speed slender body theories (von Kàrmàn 1929; Wagner 1932; Tulin 1957) to account for gravity and nonlinear free-surface effects. Ogilvie (1972) applied this approach and obtained a linear solution for the bow flow in the case of a wedge-shaped bow. Numerous authors then studied free-surface potential flow around a slender ship bow using the so-called $2\frac{1}{2}D$ or $2D+t$ theory. This approach was used to compute the flow around a flat plate placed at an angle in a uniform flow (Chapman 1975), including eventually forced periodic motions in sway and yaw (Chapman 1976), leading to good predictions of the hydrodynamic coefficients. The linearized problem was studied for both steady flow and incident head sea waves with a ship that was restrained from oscillating (Faltinsen 1983). In both cases, the bow flow solution was matched to a far-field solution representing the divergent wave system. Many comparisons were made with other measured and calculated steady wave elevation for realistic ships.

With the increase of storage and computational capacities, it became possible to solve numerically the two-dimensional nonlinear boundary value problem using the

† Present address: IFP, Institut Français du Pétrole, Division Mécanique Appliquée, 1 et 4 Avenue de Bois-Préau, 92852 Rueil-Malmaison Cedex, France.

mixed Eulerian Lagrangian (MEL) method, initially developed (independently) by Longuet-Higgins & Cokelet (1976) and Faltinsen (1977), the latter using Ogilvie's ideas. Fritts, Meinhold & Von Kerczek (1988) and Calisal & Chan (1989) applied this method and presented nonlinear numerical results for bow waves. This approach has then been used and extended to study the steady flow and the seakeeping behaviour of fast ships in the frequency domain (Faltinsen & Zhao 1991*a*, *b*; Faltinsen 1993). Time domain simulations were performed by Maruo & Song (1994), taking into account the presence of an incoming head sea wave as well as heave and pitch motion of the ship. Recently, this approach has been used to study numerically nonlinear diverging bow waves (Tulin & Wu 1996), to compute deck wetness and slamming as the bow enters an incoming wave (Wu, Fontaine & Tulin 2000), and finally to compute wave resistance either for fast ships (Fontaine & Cordier 1997) or associated with the nonlinear character of the bow waves (Zhao & Faltinsen 1999). The evolution of this theory, from a more general point of view, has recently been summarized in a review by Fontaine & Tulin (1998).

From a theoretical point of view, Fontaine & Cointe (1997) show how the method of matched asymptotic expansions can provide a consistent perturbation procedure for the justification of this approximation. To first order with respect to the slenderness parameter, the asymptotic analysis leads to the conclusion that, in the vicinity of a slender ship bow, the longitudinal perturbations of the incident uniform flow can be neglected in comparison to the transversal perturbations. In the bow domain (see figure 1), the initial steady three-dimensional nonlinear boundary value problem reduces to an unsteady two-dimensional nonlinear one. In some circumstances, the simplified two-dimensional 'parabolic' problem can moreover be linearized.

Far from the ship, the two-dimensional bow flow solution matches a three-dimensional linear far-field solution. To first order, the far-field flow does not influence the bow flow so that only the latter needs to be computed. The three-dimensional character of the bow flow is only taken into account through the free-surface conditions which lead to an interaction between successive two-dimensional cross-sections of the flow, but do not provide any upstream influence. In particular, this 'parabolic' approximation of the equations does not predict a rise of water in front of the bow, in disagreement with reality. This discrepancy between theoretical and experimental results suggests the need for a more accurate description of the flow in front of the bow. The rise of water in front could be a higher-order effect but, as we shall see, this is not the correct explanation.

In this study, a local analysis of the flow in the near-bow domain is performed leading to the determination of a near-bow solution which matches both to the bow flow and to the far-field solutions. A composite solution is then derived, which leads to an estimate of the wave elevation in front of the bow and allows a three-dimensional correction to be added to the two-dimensional solution.

The bow flow and far-field flow solutions are respectively presented in § 2 and § 3. The near-bow flow problem is then derived (§ 4) and solved analytically in the special case of a thin ship. The bow, near-bow and far-field solutions are then matched (§ 5). The asymptotic study is extended by assuming that the hull is vertical sided (§ 6). The numerical methods used in the case of a slender hull are presented (§ 7). The structure of the flow is then discussed and numerical results are presented (§ 8). Technical details associated with the asymptotic analysis are to be found in Appendices A and B.

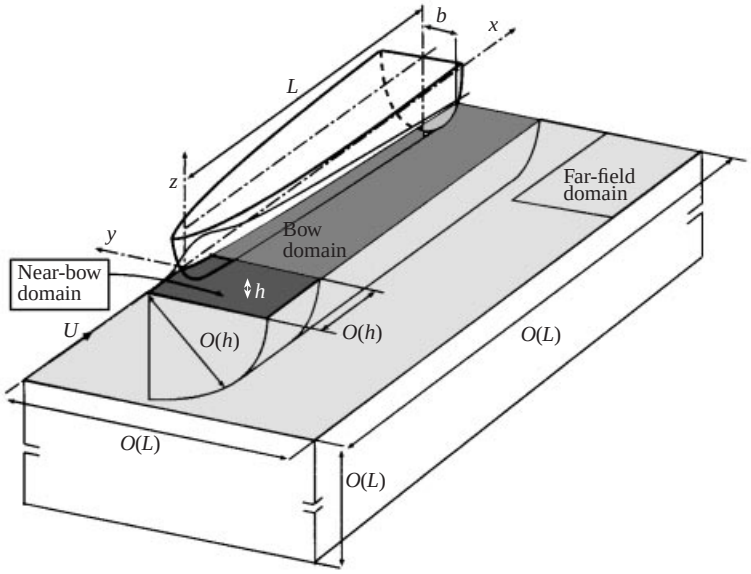

FIGURE 1. Illustration of the different domains of the composite solution.

2. The bow flow problems

The fluid is assumed to be incompressible and the flow irrotational. The ship is characterized by its maximum beam b and draught h (see figure 1). The formal equation describing the shape of the hull is $y/b = f\left(x/L, z/h\right)$ where L is the longitudinal length scale. Thus, the two non-dimensional geometrical parameters are $\tan\alpha = b/L$ and $\delta = h/L$. The ship is said to be *slender* when $\tan\alpha \simeq \delta \ll 1$ and *thin* when $\tan\alpha \ll \delta \ll 1$.

To study the flow in the vicinity of the ship, an inner (or bow) domain is defined on a radial length scale equal to the draught h and on a longitudinal length scale L. The non-dimensional variables are defined as

$$\tilde{x} = \frac{x}{L}, \quad \hat{y} = \frac{y}{h}, \quad \hat{z} = \frac{z}{h}, \quad \hat{\varphi} = \frac{\varphi}{Ub}, \quad \hat{\eta} = \frac{\eta}{b}, \tag{2.1}$$

where φ is the velocity perturbation potential and η the free-surface elevation. Assuming the ship to be slender or thin, the following asymptotic expansions are introduced:

$$\hat{\varphi}(\tilde{x}, \hat{y}, \hat{z}; \alpha, \delta) = \hat{\mu}_1(\alpha, \delta)\, \hat{\varphi}_1(\tilde{x}, \hat{y}, \hat{z}) + o(\hat{\mu}_1), \tag{2.2}$$

$$\hat{\eta}(\tilde{x}, \hat{y}; \alpha, \delta) = \hat{\nu}_1(\alpha, \delta)\, \hat{\eta}_1(\tilde{x}, \hat{y}) + o(\hat{\nu}_1), \tag{2.3}$$

where the functions $\hat{\varphi}_1, \hat{\eta}_1$ and their derivatives are assumed to be $O(1)$ and independent of α and δ if the gauge functions $\hat{\mu}_1, \hat{\nu}_1$ are correctly chosen.

2.1. *Simplified equations*

2.1.1. *Laplace equation*

Using the non-dimensional variables, the three-dimensional Laplace equation gives

$$\delta^2 \frac{\partial^2 \hat{\varphi}_1}{\partial \tilde{x}^2} + \frac{\partial^2 \hat{\varphi}_1}{\partial \hat{y}^2} + \frac{\partial^2 \hat{\varphi}_1}{\partial \hat{z}^2} + o(1) = 0 \tag{2.4}$$

and reduces, to the leading order, to its two-dimensional form in each transverse plane:

$$\frac{\partial^2 \hat{\varphi}_1}{\partial \hat{y}^2} + \frac{\partial^2 \hat{\varphi}_1}{\partial \hat{z}^2} = 0, \tag{2.5}$$

in accordance with the intuitive idea that longitudinal variations in the x-direction are small compared to the transversal ones, since the ship is slender. Obviously, three-dimensional effects that arise far from the ship cannot be described by this equation. The potential $\hat{\varphi}_1$ must therefore be interpreted as the near-field (or inner) solution.

2.1.2. *Body boundary condition*

The body boundary condition is expressed on the hull $\hat{y} = ((\tan\alpha)/\delta)\, f(\tilde{x}, \hat{z})$ and is written

$$\frac{\partial f}{\partial \tilde{x}} \left(1 + \hat{\mu}_1 \tan\alpha \frac{\partial \hat{\varphi}_1}{\partial \tilde{x}}\right) - \frac{\hat{\mu}_1}{\delta} \frac{\partial \hat{\varphi}_1}{\partial \hat{y}} + \frac{\hat{\mu}_1}{\delta} \frac{\tan\alpha}{\delta} \frac{\partial f}{\partial \hat{z}} \frac{\partial \hat{\varphi}_1}{\partial \hat{z}} + o(1) = 0. \tag{2.6}$$

Assuming the hull to be shaped, i.e. $\partial f/\partial \tilde{x} = O(1)$ and $\partial f/\partial \hat{z} = O(1)$, the principle of least degeneracy leads to $\hat{\mu}_1 = \delta$, whether the ship is thin or slender. For a slender hull ($\alpha \simeq \delta \ll 1$), the resulting condition is imposed on the exact position of the hull and reduces to

$$\left[\frac{\partial f}{\partial \tilde{x}} - \frac{\partial \hat{\varphi}_1}{\partial \hat{y}} + \frac{\tan\alpha}{\delta} \frac{\partial f}{\partial \hat{z}} \frac{\partial \hat{\varphi}_1}{\partial \hat{z}}\right] \left(\tilde{x}, \hat{y} = \frac{\tan\alpha}{\delta} f(\tilde{x}, \hat{z}), \hat{z}\right) = 0. \tag{2.7}$$

For a thin ship ($\alpha \ll \delta \ll 1$), the resulting condition can be applied on the symmetry axis of the ship without introducing any significant error at this order:

$$\left[\frac{\partial f}{\partial \tilde{x}} - \frac{\partial \hat{\varphi}_1}{\partial \hat{y}}\right] (\tilde{x}, 0, \hat{z}) = 0. \tag{2.8}$$

2.1.3. *Free-surface conditions*

The kinematic free-surface boundary condition is expressed on $\hat{z} = \hat{v}_1\, ((\tan\alpha)/\delta)\, \hat{\eta}_1$ and reads

$$\frac{\partial \hat{\eta}_1}{\partial \tilde{x}} + \delta\, \tan\alpha \frac{\partial \hat{\varphi}_1}{\partial \tilde{x}} \frac{\partial \hat{\eta}_1}{\partial \tilde{x}} + \frac{\tan\alpha}{\delta} \frac{\partial \hat{\varphi}_1}{\partial \hat{y}} \frac{\partial \hat{\eta}_1}{\partial \hat{y}} - \frac{1}{\hat{v}_1} \frac{\partial \hat{\varphi}_1}{\partial \hat{z}} + o(1) = 0. \tag{2.9}$$

The principle of least degeneracy leads to $\hat{v}_1 = 1$ in order to retain the last term of (2.9). For a slender ship, the condition (2.9) is imposed on the exact position of the free surface and reduces to

$$\left[\frac{\partial \hat{\eta}_1}{\partial \tilde{x}} + \frac{\tan\alpha}{\delta} \frac{\partial \hat{\varphi}_1}{\partial \hat{y}} \frac{\partial \hat{\eta}_1}{\partial \hat{y}} - \frac{\partial \hat{\varphi}_1}{\partial \hat{z}}\right] \left(\tilde{x}, \hat{y}, \frac{\tan\alpha}{\delta} \hat{\eta}_1\right) = 0. \tag{2.10}$$

The thin-ship assumption justifies the linearization of this condition which can then be expressed on the axis $\hat{z} = 0$:

$$\left[\frac{\partial \hat{\eta}_1}{\partial \tilde{x}} - \frac{\partial \hat{\varphi}_1}{\partial \hat{z}}\right] (\tilde{x}, \hat{y}, 0) = 0. \tag{2.11}$$

The dynamic free-surface condition gives, with $F_L^2 = U^2/gL$:

$$\frac{\partial \hat{\varphi}_1}{\partial \tilde{x}} + \frac{1}{2}\delta \tan\alpha \left(\frac{\partial \hat{\varphi}_1}{\partial \tilde{x}}\right)^2 + \frac{1}{2}\frac{\tan\alpha}{\delta}\left[\left(\frac{\partial \hat{\varphi}_1}{\partial \hat{y}}\right)^2 + \left(\frac{\partial \hat{\varphi}_1}{\partial \hat{z}}\right)^2\right] + \frac{1}{\delta F_L^2}\hat{\eta}_1 + o(1) = 0. \quad (2.12)$$

In order to find a non-trivial solution for $\hat{\eta}_1$, it is necessary to impose

$$\hat{F}_L^2 = \frac{\delta U^2}{gL} \geqslant O(1). \quad (2.13)$$

For a slender ship, the dynamic free-surface condition then reduces to

$$\left[\frac{\partial \hat{\varphi}_1}{\partial \tilde{x}} + \frac{1}{2}\frac{\tan\alpha}{\delta}\left(\left(\frac{\partial \hat{\varphi}_1}{\partial \hat{y}}\right)^2 + \left(\frac{\partial \hat{\varphi}_1}{\partial \hat{z}}\right)^2\right)\right]\left(\tilde{x}, \hat{y}, \frac{\tan\alpha}{\delta}\hat{\eta}_1\right) + \frac{\hat{\eta}_1}{\hat{F}_L^2} = 0. \quad (2.14)$$

When the ship is thin, the resulting dynamic free-surface boundary condition is linear:

$$\left[\frac{\partial \hat{\varphi}_1}{\partial \tilde{x}} + \frac{1}{\hat{F}_L^2}\hat{\eta}_1\right](\tilde{x}, \hat{y}, 0) = 0. \quad (2.15)$$

In this case, the free-surface conditions (2.11) and (2.15) can be rearranged to give the classical Neumann–Kelvin condition for the potential:

$$\left[\frac{\partial^2 \hat{\varphi}_1}{\partial \tilde{x}^2} + K\frac{\partial \hat{\varphi}_1}{\partial \hat{z}}\right](\tilde{x}, \hat{y}, 0) = 0, \quad \text{with} \quad K = \frac{1}{\delta F_L^2} \leqslant O(1). \quad (2.16)$$

2.2. *Asymptotic domain of validity*

To summarize, the flow in the vicinity of a slender hull is governed to first order by the two-dimensional Laplace equation (2.5) subject to the boundary conditions (2.7), (2.10) and (2.14). These equations also apply when the ship is assumed to be thin, but in this last case the boundary conditions can moreover be linearized to give (2.8) and (2.16). Apart from the slender ship hypothesis, the main assumption leading to the asymptotic expansion is given by the condition (2.13) on the Froude number.

If L is the length of the ship, this equation implies that U must satisfy

$$F_L = \frac{U}{(g\,L)^{1/2}} \geqslant O\left(\frac{1}{\delta^{1/2}}\right) = O\left(\left(\frac{L}{h}\right)^{1/2}\right). \quad (2.17)$$

This confirms that these asymptotic equations can be applied to study the flow around slender high-speed ships. When the Froude number is much larger than $1/\delta^{1/2}$, the effects of gravity can be neglected. This case corresponds in practice to the flow around a planing hull.

Even for slower ships, this approximation applies to a distance L from the bow if L is chosen so that

$$L \leqslant O\left(U\left(\frac{h}{g}\right)^{1/2}\right) = O(h\,F_h), \quad \text{where} \quad F_h = \frac{U}{(gh)^{1/2}}. \quad (2.18)$$

This expression gives the order of magnitude of L for the approximation to remain valid, as long as the ship is assumed to be slender or thin. These hypotheses require that $F_h \gg O(1)$. These simplified equations can therefore be applied to study the flow around the bow of a slender ship if the Froude number based on the draught is high enough.

3. The far-field flow

The bow flow solution only satisfies the two-dimensional Laplace equation and is therefore not valid far from the ship. Boundary conditions at infinity, for the bow flow problem, must be provided by a matching condition with a far-field (or outer) solution. The far-field domain is defined on the length scale L so that the outer variables are defined as

$$\tilde{y} = \frac{y}{L} = \delta\,\hat{y}, \quad \tilde{z} = \frac{z}{L} = \delta\,\hat{z}, \quad \tilde{\eta} = \hat{\eta}, \quad \tilde{\varphi} = \hat{\varphi}, \tag{3.1}$$

and the following asymptotic expansions are performed:

$$\tilde{\varphi}(\tilde{x},\tilde{y},\tilde{z};\alpha,\delta) = \tilde{\mu}_1(\alpha,\delta)\,\tilde{\varphi}_1(\tilde{x},\tilde{y},\tilde{z}) + o(\tilde{\mu}_1), \tag{3.2}$$

$$\tilde{\eta}(\tilde{x},\tilde{y};\alpha,\delta) = \tilde{v}_1(\alpha,\delta)\,\hat{\eta}_1(\tilde{x},\tilde{y}) + o(\tilde{v}_1). \tag{3.3}$$

Since in the far-field domain the space variables are not stretched, the leading-order perturbation potential $\tilde{\varphi}_1$ satisfies the three-dimensional Laplace equation in the fluid domain. From the far-field point of view, the details of the hull shape cannot be distinguished, so that the hull appears as a straight line segment $[0,1]$ along the $\tilde{x}$-axis. The body boundary condition is thus replaced by a matching condition with the bow flow solution. Using the outer variables, the free-surface conditions give

$$\frac{\partial\tilde{\eta}_1}{\partial\tilde{x}} + \tilde{\mu}_1\tan\alpha\left(\frac{\partial\tilde{\varphi}_1}{\partial\tilde{x}}\frac{\partial\tilde{\eta}_1}{\partial\tilde{x}} + \frac{\partial\tilde{\varphi}_1}{\partial\tilde{y}}\frac{\partial\tilde{\eta}_1}{\partial\tilde{y}}\right) - \frac{\tilde{\mu}_1}{\tilde{v}_1}\frac{\partial\tilde{\varphi}_1}{\partial\tilde{z}} + o(1) = 0, \tag{3.4}$$

$$\frac{\partial\tilde{\varphi}_1}{\partial\tilde{x}} + \frac{1}{2}\,\tilde{\mu}_1\tan\alpha\left(\left(\frac{\partial\tilde{\varphi}_1}{\partial\tilde{x}}\right)^2 + \left(\frac{\partial\tilde{\varphi}_1}{\partial\tilde{y}}\right)^2 + \left(\frac{\partial\tilde{\varphi}_1}{\partial\tilde{z}}\right)^2\right) + \frac{\tilde{v}_1}{\tilde{\mu}_1 F_L^2}\,\tilde{\eta}_1 + o(1) = 0. \tag{3.5}$$

The simplified free-surface conditions are obtained using the principle of least degeneracy (see Fontaine 1996 for the details), leading to

$$\frac{\partial\tilde{\varphi}_1}{\partial\tilde{x}}(\tilde{x},\tilde{y},0) = 0, \tag{3.6}$$

$$\left[\frac{\partial\tilde{\eta}_1}{\partial\tilde{x}} - \frac{\partial\tilde{\varphi}_1}{\partial\tilde{z}}\right](\tilde{x},\tilde{y},0) = 0. \tag{3.7}$$

The potential must therefore vanish on the undisturbed free surface ($\tilde{z} = 0$), except in the wake of the ship, i.e. $\tilde{y} = \tilde{z} = 0,\ \tilde{x} > 1$, where it can be constant. The general far-field solution is expressed as a multipole expansion (Ward 1955). Matching this solution to the bow flow solution leads to the conclusion that $\tilde{\mu}_1 = \tilde{v}_1 = \delta^2$ and

$$\tilde{\varphi}_1(\tilde{x},\tilde{r},\theta) = \int_0^\infty \frac{-\mu(s)}{4\,\pi}\,\frac{\tilde{r}\,\sin(\theta)}{\left[(\tilde{x}-s)^2+\tilde{r}^2\right]^{3/2}}\,\mathrm{d}s, \tag{3.8}$$

where $\theta = \arctan(\tilde{z}/\tilde{y})$ and $\tilde{r} = (\tilde{y}^2+\tilde{z}^2)^{1/2}$. The far-field solution is thus given by a distribution of three-dimensional vertical dipoles on the axis $\tilde{x} \geqslant 0$. In order to satisfy the outer dynamic free-surface condition, the dipole density μ must be constant, equal to μ_w in the wake behind the ship, which leads to

$$\tilde{\varphi}_1 = \int_0^1 -\frac{\mu(s)}{4\pi}\,\frac{\tilde{r}\,\sin(\theta)}{\left[(\tilde{x}-s)^2+\tilde{r}^2\right]^{3/2}}\,\mathrm{d}s - \frac{\mu_w}{4\pi}\,\frac{\sin(\theta)}{\tilde{r}}\left(1 + \frac{\tilde{x}-1}{\sqrt{(\tilde{x}-1)^2+\tilde{r}^2}}\right), \tag{3.9}$$

$$\tilde{\eta}_1 = \frac{1}{\tilde{y}^2}\int_0^1 -\frac{\mu(s)}{4\pi}\left[1+\frac{\tilde{x}-s}{\sqrt{(\tilde{x}-s)^2+\tilde{y}^2}}\right]\mathrm{d}s - \frac{\mu_w}{4\pi\,\tilde{y}^2}\left[\tilde{x}-1+\sqrt{(\tilde{x}-1)^2+\tilde{y}^2}\right]. \tag{3.10}$$

The dipole density $\mu(\tilde{x})$ is deduced from the behaviour of the bow flow solution. Far from the hull, as $\hat{r} = \tilde{r}/\delta \to +\infty$, the bow flow potential behaves like a two-dimensional vertical dipole whose density is equal to the three-dimensional dipole density of the outer solution:

$$\lim_{\hat{r}\to\infty} \hat{\varphi}_1(\tilde{x},\hat{r},\theta) = -\frac{\mu(\tilde{x})}{2\pi}\frac{\sin(\theta)}{\hat{r}}. \tag{3.11}$$

Since the outer solution (3.8) is regular in front of the ship ($\tilde{x} < 0$), the initial conditions for the bow flow problem may be found by matching the bow flow and far-field flow solutions. The behaviour of the far-field potential near the origin is derived in Appendix B. The inner expansion of the far-field solution appears to be an order of magnitude smaller than the outer expansion of the bow flow solution. To overcome this mis-match, we look for an asymptotic expansion of the solution in the near-bow domain. The near-bow flow solution is then matched to the bow flow solution and to the far-field solution.

4. The near-bow flow

The near-bow domain is defined on a length scale equal to h so that the following additional non-dimensional variables are defined:

$$\hat{x} = \frac{x}{h}, \quad \breve{\varphi} = \hat{\varphi}, \quad \breve{\eta} = \hat{\eta}. \tag{4.1}$$

Assuming the ship bow to be thin or slender, the following asymptotic expansions are performed:

$$\breve{\varphi}(\hat{x},\hat{y},\hat{z};\alpha,\delta) = \breve{\mu}_1(\alpha,\delta)\,\breve{\varphi}_1(\hat{x},\hat{y},\hat{z}) + o(\breve{\mu}_1), \tag{4.2}$$

$$\breve{\eta}(\hat{x},\hat{y};\alpha,\delta) = \breve{\nu}_1(\alpha,\delta)\,\breve{\eta}_1(\hat{x},\hat{y}) + o(\breve{\nu}_1). \tag{4.3}$$

4.1. *Simplified equations*

Since in the near-bow domain the space variables are not stretched, the leading-order perturbation potential $\breve{\varphi}_1$ satisfies the three-dimensional Laplace equation in the fluid domain:

$$\frac{\partial^2\breve{\varphi}_1}{\partial\hat{x}^2} + \frac{\partial^2\breve{\varphi}_1}{\partial\hat{y}^2} + \frac{\partial^2\breve{\varphi}_1}{\partial\hat{z}^2} = 0, \tag{4.4}$$

subject to the following boundary conditions.

4.1.1. *Body boundary condition*

$$\left(1+\breve{\mu}_1\frac{\tan\alpha}{\delta}\frac{\partial\breve{\varphi}_1}{\partial\hat{x}}\right)\frac{\partial f}{\partial\tilde{x}} - \frac{\breve{\mu}_1}{\delta}\frac{\partial\breve{\varphi}_1}{\partial\hat{y}} + \breve{\mu}_1\frac{\tan\alpha}{\delta^2}\frac{\partial\breve{\varphi}_1}{\partial\hat{z}}\frac{\partial f}{\partial\hat{z}} + o(1) = 0. \tag{4.5}$$

The principle of least degeneracy enables one to conclude that $\breve{\mu}_1 = \delta$ for both a slender and a thin ship. The perturbation potential is of the same order of magnitude in the near-bow domain as in the bow domain. Consequently, the transversal components of the velocity perturbation have the same order of magnitude in the two domains. However the longitudinal component, i.e. in the x-direction, is an order of magnitude

bigger in the near-bow domain than in the bow one. When the ship is slender, the resulting body boundary condition is

$$\frac{\partial f}{\partial \tilde{x}} - \frac{\partial \breve{\varphi}_1}{\partial \hat{y}} + \frac{\tan\alpha}{\delta}\frac{\partial f}{\partial \hat{z}}\frac{\partial \breve{\varphi}_1}{\partial \hat{z}} = 0 \quad \text{on} \quad \hat{y} = \frac{\tan\alpha}{\delta} f(\tilde{x}, \hat{z}). \tag{4.6}$$

When the ship is thin, the resulting boundary condition can be further simplified and applies on the centre-plane of the hull:

$$\frac{\partial f}{\partial \tilde{x}} - \frac{\partial \breve{\varphi}_1}{\partial \hat{y}} = 0 \quad \text{on} \quad \hat{y} = 0. \tag{4.7}$$

4.1.2. *Free-surface conditions*

Using the previous result for the order of magnitude of the potential, the kinematic free-surface condition gives

$$\left(1 + \tan\alpha \frac{\partial \breve{\varphi}_1}{\partial \hat{x}}\right)\frac{\partial \breve{\eta}_1}{\partial \hat{x}} + \tan\alpha \frac{\partial \breve{\varphi}_1}{\partial \hat{y}}\frac{\partial \breve{\eta}_1}{\partial \hat{y}} - \frac{\delta}{\breve{v}_1}\frac{\partial \breve{\varphi}_1}{\partial \hat{z}} + o(1) = 0. \tag{4.8}$$

The principle of least degeneracy leads to $\breve{v}_1 = \delta$ and the resulting simplified kinematic free-surface condition is linear:

$$\frac{\partial \breve{\eta}_1}{\partial \hat{x}} - \frac{\partial \breve{\varphi}_1}{\partial \hat{z}} = 0 \quad \text{on} \quad \hat{z} = 0. \tag{4.9}$$

The dynamic free-surface condition gives

$$\frac{\partial \breve{\varphi}_1}{\partial \hat{x}} + \frac{1}{2}\tan\alpha\left(\left(\frac{\partial \breve{\varphi}_1}{\partial \hat{x}}\right)^2 + \left(\frac{\partial \breve{\varphi}_1}{\partial \hat{y}}\right)^2 + \left(\frac{\partial \breve{\varphi}_1}{\partial \hat{z}}\right)^2\right) + \tan\alpha \frac{gL}{U^2}\breve{\eta}_1 + o(1) = 0 \quad \text{on} \quad \hat{z} = 0. \tag{4.10}$$

From (2.13), it follows that $gL/U^2 \leqslant \delta \ll 1$ so that $\tan\alpha\, gL/U^2 \ll \tan\alpha \ll 1$. As a result, the last term of (2.14) is of higher order and can be dropped. Assuming the perturbation potential vanishes at infinity in front of the ship ($\hat{x} \to -\infty$), the resulting simplified dynamic free-surface condition is

$$\breve{\varphi}_1(\hat{x}, \hat{y}, 0) = 0. \tag{4.11}$$

To first order, gravity effects can be neglected in front of the bow and free-surface particles have only a vertical velocity. The near-bow flow problem is thus similar to a typical impact problem, see Cointe (1989).

4.2. *Near-bow flow solution for a thin ship*

In the near-bow domain, the perturbation potential satisfies the three-dimensional Laplace equation and vanishes on the undisturbed free surface. When the ship is slender, the body boundary condition applies to the exact position of the hull and the near-bow flow problem must, in general, be solved numerically (see § 7). In order to gain some insight into the structure of the solution, the ship bow is assumed to be thin. This assumption allows an analytical solution to be found since the near-bow flow potential can be expressed in term of a distribution of sources and sinks on the centre-plane of the hull and its mirror image. For the sake of simplicity, the draught of the ship is assumed to be constant so that the solution is then given by

$$\breve{\varphi}_1 = \lim_{\delta \to 0} \frac{1}{2\pi}\int_{-1}^{0} \mathrm{d}\zeta \int_{0}^{L/\delta} f_{\tilde{x}}(\delta\xi, \zeta)\, G(\hat{x}, \hat{y}, \hat{z}, \xi, \zeta)\, \mathrm{d}\xi \tag{4.12}$$

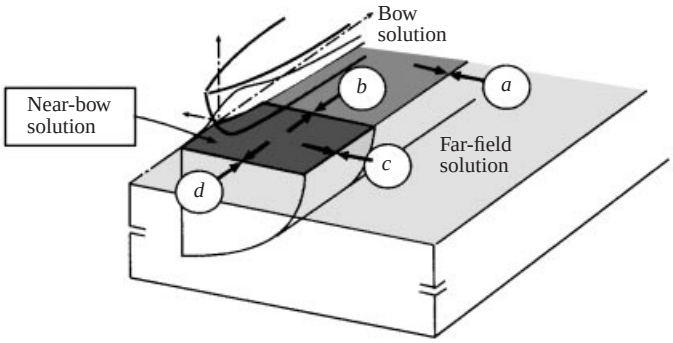

FIGURE 2. Illustration of the matching processes.

with

$$G = \left[(\hat{x}-\xi)^2 + \hat{y}^2 + (\hat{z}+\zeta)^2\right]^{-1/2} - \left[(\hat{x}-\xi)^2 + \hat{y}^2 + (\hat{z}-\zeta)^2\right]^{-1/2}. \tag{4.13}$$

Performing the integration and taking the limit leads to

$$\breve{\varphi}_1 = \frac{1}{2\pi}\int_{-1}^{0} f_{\tilde{x}}(0,\zeta)\,\ln\left[\frac{-\hat{x}+\left(\hat{x}^2+\hat{y}^2+(\hat{z}-\zeta)^2\right)^{1/2}}{-\hat{x}+\left(\hat{x}^2+\hat{y}^2+(\hat{z}+\zeta)^2\right)^{1/2}}\right]\mathrm{d}\zeta. \tag{4.14}$$

It is easy to check that the homogeneous Dirichlet condition (4.11) is satisfied on the undisturbed free surface, and it is also shown in Appendix A that the linearized body boundary condition (4.7) is met.

5. Matching of the solutions

The matching procedure is illustrated in figure 2. The matching (*a*), between the bow and far-field solution is given in Fontaine & Cointe (1997). Here, we have to check that the near-bow solution matches on the one hand the bow solution (*b*) and on the other hand the far-field solution (*c*) and (*d*).

5.1. *Matching near-bow flow and the bow flow solutions*

In order to match the near-bow flow solution to the bow flow one, we follow Kevorkian & Cole (1981) and define an intermediate variable $x_\chi = \tilde{x}/\chi(\delta)$, with $\delta \ll \chi(\delta) \ll 1$, which is $O(1)$ in the overlap domain. The matching condition at first order is then

$$\lim_{\substack{\delta\to 0\\ x_\chi = O(1)\\ x_\chi>0}} \frac{1}{\delta}\left[\delta\,\breve{\varphi}_1\left(\frac{\chi(\delta)}{\delta}x_\chi,\hat{y},\hat{z}\right) - \delta\,\hat{\varphi}_1(\chi(\delta)x_\chi,\hat{y},\hat{z})\right] = 0. \tag{5.1}$$

The first term of this equation describes the behaviour of the near-bow flow solution as $\hat{x}\to+\infty$ and can easily be derived from equation (4.14):

$$\lim_{\substack{\delta\to 0\\ x_\chi = O(1)\\ x_\chi>0}} \breve{\varphi}_1\left(\frac{\chi(\delta)}{\delta}x_\chi,\hat{y},\hat{z}\right) = \frac{1}{2\pi}\int_{-1}^{0} f_{\tilde{x}}(0,\zeta)\,\ln\left[\frac{\hat{y}^2+(\hat{z}-\zeta)^2}{\hat{y}^2+(\hat{z}+\zeta)^2}\right]\mathrm{d}\zeta + O\left[\left(\frac{\delta}{\chi(\delta)}\right)^2\right]. \tag{5.2}$$

Since this quantity is $O(1)$, the bow flow and the near-bow flow solutions have the same order of magnitude in the overlap domain. According to (5.1), the bow flow

solution is matched to the near-bow flow solution if

$$\hat{\varphi}_1(0,\hat{y},\hat{z}) = \frac{1}{2\pi}\int_{-1}^{0} f_{\tilde{x}}(0,\zeta)\,\ln\left[\frac{\hat{y}^2+(\hat{z}-\zeta)^2}{\hat{y}^2+(\hat{z}+\zeta)^2}\right]\mathrm{d}\zeta. \tag{5.3}$$

This condition is satisfied if the initial conditions for the bow flow problem are

$$\hat{\varphi}_1(0,\hat{y},0) = 0 \quad \text{and} \quad \hat{\eta}_1(0,\hat{y}) = 0. \tag{5.4}$$

The matching conditions (5.1) between the bow flow and near-bow flow solutions allow therefore the justification of the classical closure assumptions (5.4) used to compute the bow flow solution. The bow flow solution is therefore a fully two-dimensional solution and does not include any upstream influence between the strips. We will show in the next section how three-dimensional effects arise in the composite solution.

5.2. *Matching near-bow flow and the far-field flow solutions*

In order to perform this matching, we have to check that the two solutions match in two limit processes. The two solutions must match far from the side of the bow, i.e. $\hat{x} = O(1)$ and $\hat{r} \to +\infty$, and in front of the ship, i.e. $\hat{r} = O(1)$ and $\hat{x} \to -\infty$.

5.2.1. *First limit process:* $\hat{x} = O(1)$ *and* $\hat{r} \to +\infty$

As before, we define an intermediate variable $r_\chi = \tilde{r}/\chi(\delta)$, with $\delta \ll \chi(\delta) \ll 1$, which is $O(1)$ in the overlap domain. To first order, the matching condition is

$$\lim_{\substack{\delta\to 0\\ r_\chi = O(1)}} \frac{1}{\delta}\left[\delta\,\breve{\varphi}_1\left(\hat{x},\frac{\chi(\delta)}{\delta}r_\chi,\theta\right) - \delta^2\,\tilde{\varphi}_1(\delta\hat{x},\chi(\delta)r_\chi,\theta)\right] = 0. \tag{5.5}$$

The first term of this equation describes the behaviour of the near-bow flow solution far from the side of the ship bow, as $\hat{r} \to +\infty$, and can be evaluated using (4.14). The second term of this equation describes the behaviour of the far-field solution near to the side of the ship, i.e. as $\tilde{r} \to 0$, and can be derived from (3.8). The details of these calculations may be found in Appendix B. This leads to

$$\lim_{\substack{\delta\to 0\\ r_\chi = O(1)}} \delta\,\breve{\varphi}_1\left(\hat{x},\frac{\chi(\delta)}{\delta}r_\chi,\theta\right) = -\frac{\delta^2}{\chi(\delta)}\frac{\sin\theta}{r_\chi}\frac{1}{\pi}\int_{-1}^{0}\zeta\,f_{\tilde{x}}(0,\zeta)\,\mathrm{d}\zeta + O\left[\frac{\delta^3}{\chi(\delta)^2}\right], \tag{5.6}$$

$$\lim_{\substack{\delta\to 0\\ r_\chi = O(1)}} \delta^2\tilde{\varphi}_1(\delta\hat{x},\chi(\delta)r_\chi,\theta) = -\frac{\delta^2}{\chi(\delta)}\frac{\sin\theta}{r_\chi}\frac{\mu(0)}{4\pi} + o\left[\frac{\delta^2}{\chi(\delta)}\right]. \tag{5.7}$$

The dipole density at the origin $\mu(0)$ is obtained from (3.11) by analysing the behaviour of the bow flow solution for $\tilde{x} = 0$ and $\hat{r} \to +\infty$. Using (5.3), it follows that

$$\lim_{\hat{r}\to+\infty} \hat{\varphi}_1(0,\hat{r},\theta) = -\frac{2}{\pi}\frac{\sin\theta}{\hat{r}}\int_{-1}^{0}\zeta\,f_{\tilde{x}}(0,\zeta)\,\mathrm{d}\zeta + O\left(\frac{1}{\hat{r}^3}\right). \tag{5.8}$$

Substituting this expression into (3.11) finally gives

$$\mu(0) = 4\int_{-1}^{0}\zeta\,f_{\tilde{x}}(0,\zeta)\,\mathrm{d}\zeta, \tag{5.9}$$

so that the matching condition (5.5) is satisfied.

5.2.2. *Second limit process:* $\hat{r} = O(1)$ *and* $\hat{x} \to -\infty$

We define an intermediate variable $x_\chi = \tilde{x}/\chi(\delta)$, with $\delta \ll \chi(\delta) \ll 1$, which is $O(1)$ in the overlap domain. To first order, the matching condition is

$$\lim_{\substack{\delta\to 0\\ x_\chi = O(1)\\ x_\chi<0}} \frac{1}{\breve{\mu}_1}\left[\breve{\mu}_1\breve{\varphi}_1\left(\frac{\chi(\delta)}{\delta}x_\chi, \hat{r}, \theta\right) - \tilde{\mu}_1\tilde{\varphi}_1\left(\chi(\delta)x_\chi, \delta\hat{r}, \theta\right)\right] = 0. \tag{5.10}$$

The first term of this equation describes the behaviour of the near-bow flow solution in front of the ship bow, as $\hat{x} \to -\infty$, and can be evaluated using (4.14). The second term in the matching condition describes the behaviour of the far-field flow solution in front of the ship bow as $\tilde{x} \to 0^-$, and can be obtained from (3.8). The details of these calculations may be found in Appendix B. This leads to

$$\lim_{\substack{\delta\to 0\\ x_\chi = O(1)\\ x_\chi<0}} \delta\breve{\varphi}_1\left(\frac{\chi(\delta)}{\delta}x_\chi, \hat{r}, \theta\right) = -\frac{1}{2\pi}\frac{\delta^3}{\chi(\delta)^2}\frac{\hat{r}\sin\theta}{{x_\chi}^2}\int_{-1}^{0}\zeta\, f_{\tilde{x}}(0,\zeta)\,\mathrm{d}\zeta + o\left[\frac{\delta^3}{\chi(\delta)^2}\right], \tag{5.11}$$

$$\lim_{\substack{\delta\to 0\\ x_\chi = O(1)\\ x_\chi<0}} \delta^2\,\tilde{\varphi}_1(\chi(\delta)x_\chi, \delta\hat{r}, \theta) = -\frac{\delta^3}{\chi(\delta)^2}\frac{\mu(0)}{8\pi}\frac{\hat{r}\sin\theta}{x_\chi^2} + o\left[\frac{\delta^3}{\chi(\delta)^2}\right]. \tag{5.12}$$

Substituting the value of $\mu(0)$ from (5.9) in this last equation leads to the conclusion that the two solutions match.

5.3. *Composite solution for the potential*

The perturbation potential is given by

$$\frac{\varphi}{Ub} = \begin{cases} \delta\,\breve{\varphi}_1(\hat{x},\hat{y},\hat{z}) & \text{in the near-bow domain}\\ \delta\,\hat{\varphi}_1(\tilde{x},\hat{y},\hat{z}) & \text{in the bow domain}\\ \delta^2\,\tilde{\varphi}_1(\tilde{x},\tilde{y},\tilde{z}) & \text{in the far-field domain.}\end{cases} \tag{5.13}$$

Near the ship, a composite solution can be obtained by adding the near-bow flow solution to the bow flow solution and by subtracting the common part of the two expansions. For the potential, the common part is given by (5.3). Since the bow flow solution vanishes in front of the bow ($\tilde{x} \leqslant 0$), the composite solution around the bow ($\hat{r} = O(1)$) is given by

$$\frac{\varphi}{Ub} = \begin{cases} \delta\,\breve{\varphi}_1(\hat{x},\hat{y},\hat{z}) & \text{for}\quad \hat{x} < 0\\ \delta\left[\hat{\varphi}_1 + \breve{\varphi}_1 - \dfrac{1}{2\pi}\displaystyle\int_{-1}^{0} f_{\tilde{x}}(0,\zeta)\,\ln\left(\frac{\hat{y}^2+(\hat{z}-\zeta)^2}{\hat{y}^2+(\hat{z}+\zeta)^2}\right)\mathrm{d}\zeta\right] & \text{for}\quad \hat{x} \geqslant 0.\end{cases} \tag{5.14}$$

6. Special case of a vertical sided hull

In general, the near-bow solution (4.14) requires knowledge of the hull shape at the edge of the thin ship bow. The asymptotic analysis can be further extended by considering the special case of a vertical sided hull for which $f_{\tilde{x}}(0,\xi)$ is constant. In the near-bow domain, the hull is then approximated to first order by an infinitely long wedge with constant draught h and an apex angle equal to 2α. This flow has been studied by Fontaine & Faltinsen (1997).

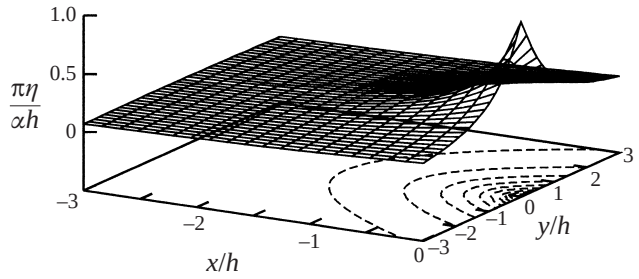

FIGURE 3. Free-surface elevation in front of the thin vertical-sided hull.

6.1. *Near-bow free-surface elevation*

In the near-bow domain, the vertical velocity of the free surface can be evaluated using (4.14), so that the kinematic free-surface condition (4.9) becomes

$$\begin{aligned}\frac{\partial\breve{\eta}_1}{\partial\hat{x}} &= -\frac{1}{\pi}\int_{-1}^{0}\frac{s}{\left(-\hat{x}+(\hat{x}^2+\hat{y}^2+s^2)^{1/2}\right)\,(\hat{x}^2+\hat{y}^2+s^2)^{1/2}}\,\mathrm{d}s\\ &= -\frac{1}{\pi}\left[\ln\left(-\hat{x}+(\hat{x}^2+\hat{y}^2+s^2)^{1/2}\right)\right]_{-1}^{0}\\ &= -\frac{1}{\pi}\ln\left[\frac{-\hat{x}+(\hat{x}^2+\hat{y}^2)^{1/2}}{-\hat{x}+(\hat{x}^2+\hat{y}^2+1)^{1/2}}\right].\end{aligned} \tag{6.1}$$

An explicit solution for $\breve{\eta}_1$ can be found by partial integration of this last equation, assuming that $\breve{\eta}_1 \to 0$ as $\hat{x} \to -\infty$:

$$\begin{aligned}\breve{\eta}_1(\hat{x},\hat{y}) &= \int_{-\infty}^{\hat{x}}\frac{\partial\breve{\eta}_1}{\partial s}\,\mathrm{d}s\\ &= -\frac{1}{\pi}\left[s\ln\left(\frac{-s+\left(s^2+\hat{y}^2\right)^{1/2}}{-s+\left(s^2+\hat{y}^2+1\right)^{1/2}}\right)+(s^2+\hat{y}^2)^{1/2}-(s^2+\hat{y}^2+1)^{1/2}\right]_{-\infty}^{\hat{x}}\\ &= -\frac{1}{\pi}\left[\hat{x}\ln\left(\frac{-\hat{x}+(\hat{x}^2+\hat{y}^2)^{1/2}}{-\hat{x}+(\hat{x}^2+\hat{y}^2+1)^{1/2}}\right)+(\hat{x}^2+\hat{y}^2)^{1/2}-(\hat{x}^2+\hat{y}^2+1)^{1/2}\right].\end{aligned} \tag{6.2}$$

This expression is plotted in figure 3 and shows the formation of a hump in front of the bow.

6.2. *Composite solution for the free-surface elevation*

Since the bow solution vanishes for $\hat{x} < 0$, the composite solution for the wave elevation is equal to the near-bow solution given by (6.2). Along the hull, i.e. for $\hat{x} \geqslant 0$, the composite solution is obtained by adding the correction $\Delta\hat{\eta}_1$ to the bow solution:

$$\frac{\eta}{b} \simeq \begin{cases}\delta\,\breve{\eta}_1(\hat{x},\hat{y},\hat{z}) & \text{for} \quad \hat{x}<0\\ \hat{\eta}_1+\Delta\hat{\eta}_1 & \text{for} \quad \hat{x}\geqslant 0.\end{cases} \tag{6.3}$$

By construction of the composite solution, this correction is equal to the difference between the near-bow flow elevation and the common part of the two asymptotic

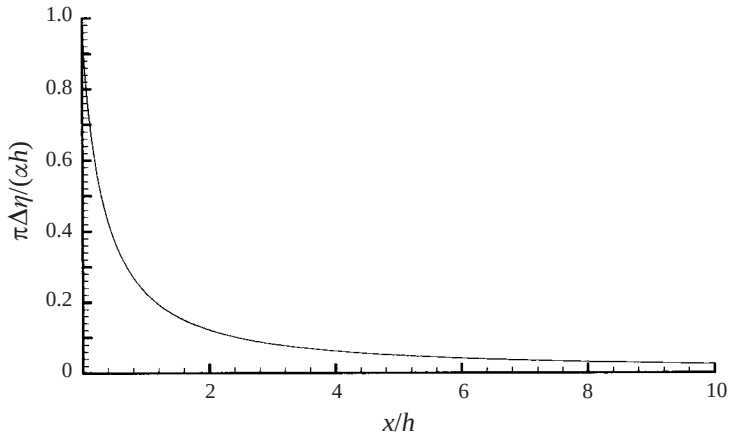

FIGURE 4. Three-dimensional correction to be added to the two-dimensional bow solution.

expansions of the free-surface elevation:

$$\Delta\hat{\eta}_1 = \delta \int_{-\infty}^{\hat{x}} -\frac{1}{\pi} \ln\left[\frac{-s+(s^2+\hat{y}^2)^{1/2}}{-s+(s^2+\hat{y}^2+1)^{1/2}}\right] \mathrm{d}s + \delta \int_0^{\hat{x}} \frac{1}{\pi} \ln\left(\frac{\hat{y}^2}{\hat{y}^2+1}\right) \mathrm{d}s. \quad (6.4)$$

The last term of this equation represents the common part of the two expansions for the free-surface elevation. It is equal to the derivative with respect to the variable $\hat{z}$ of the common part of the expansions for the potential (5.3), evaluated on the undisturbed free surface ($\hat{z} = 0$). Performing the integrals leads to the following three-dimensional correction for $x \geqslant 0$:

$$\frac{\Delta\hat{\eta}_1}{\delta} = -\frac{1}{\pi}\left[\hat{x}\ln\left(\frac{(-\hat{x}+(\hat{x}^2+\hat{y}^2)^{1/2})}{(-\hat{x}+(\hat{x}^2+\hat{y}^2+1)^{1/2})}\frac{(\hat{y}^2+1)}{\hat{y}^2}\right)+(\hat{x}^2+\hat{y}^2)^{1/2}-(\hat{x}^2+\hat{y}^2+1)^{1/2}\right]. \quad (6.5)$$

The three-dimensional correction for the wave profile along the thin hull is obtained by taking the limit of this expression as $\hat{y} \to 0$, leading to

$$\Delta\eta = b\,\Delta\hat{\eta}_1(\hat{x},0) = \frac{\alpha h}{\pi}\left[\hat{x}\ln\left(2\hat{x}(-\hat{x}+(\hat{x}^2+1)^{1/2})\right) - \hat{x} + (\hat{x}^2+1)^{1/2}\right]. \quad (6.6)$$

This expression is plotted in figure 4 which shows that the correction decays rapidly to zero (as $O(1/\hat{x})$) far from the bow edge, so that the composite solution differs from the bow solution only in the neighbourhood of the edge of the bow.

7. Numerical simulations

In the previous sections, an analytic framework for describing the surface displacement around a thin ship bow has been derived, leading to some insight into the structure of the flow. The thin ship approximation, initially introduced by Michell (1898) in a pioneering work, suffers however from a lack of precision, largely because ships are not sufficiently thin. In the more general case of a slender ship, the near-bow, bow flow and composite solutions have to be computed numerically. After describing briefly the numerical methods used, we present comparisons with experiments to show how the results relate to the physical context.

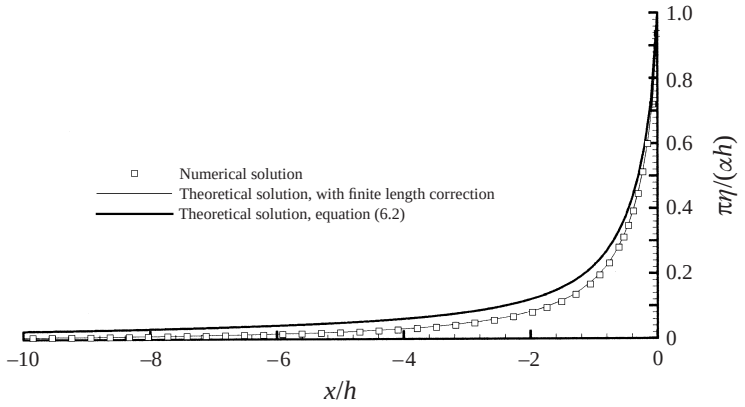

FIGURE 5. Comparison between numerical and theoretical solution for the wave elevation in front of the wedge-shaped bow along the line $\hat{y} = 0$.

7.1. *The near-bow flow solution*

To compute the near-bow flow solution, the three-dimensional Laplace equation (4.4) is solved using a classical panel method based on Rankine singularities (see Delhommeau 1987). The solution is expressed as a distribution of sources placed on the exact position of the hull and associated sinks on its mirror image with respect to the free surface. The dynamic free surface (4.11) is therefore automatically enforced. The density of the singularities is computed through the resolution of an integral equation and using the boundary condition on the hull (4.6). Finally, the free-surface condition (4.9) is integrated numerically using a standard time-stepping procedure, such as the fourth-order Runge–Kutta algorithm. The numerical program has been verified by comparison with the analytical results corresponding to the thin-ship approximation (see figure 5). In order to reach a satisfactory agreement between numerical and theoretical results, it has been found necessary to account for the finite length of the ship. The theoretical solution for the free-surface elevation in front of thin ship, (6.2), has been computed analytically taking into account the finite value of δ. A sink was also placed at the stern so that the net flux of water over the surface of the wedge is exactly zero. With these precautions, it was shown that the numerical solution converges to the analytical one as the wedge angle goes to zero.

7.2. *The bow flow solution*

An interesting way of interpreting the bow-flow problem is to consider a frame of reference fixed with respect to the fluid. Through the relationship $x = Ut$, the ship can be seen as a two-dimensional deformable wavemaker. The two-dimensional bow flow appears to be generated by the change of area of the section of the ship in the cross-plane, leading to the generation and propagation of nonlinear diverging waves. To solve numerically the bow flow problem, we use a mixed Eulerian Lagrangian method (MEL) similar to that introduced by Longuet-Higgins & Cokelet (1976) based on the Sindbad code (Cointe 1990). Details of the numerical method can be found in Fontaine (1996) and Fontaine & Cointe (1997) so that only key ideas will be given here.

The nonlinear free-surface conditions (2.10) and (2.14) are expressed in a Lagrangian form

$$\frac{\mathrm{D}\varphi}{\mathrm{D}t} = -g\,z + \frac{1}{2}\left[\left(\frac{\partial\varphi}{\partial s}\right)^2 + \left(\frac{\partial\varphi}{\partial n}\right)^2\right], \tag{7.1}$$

$$\frac{\mathrm{D}\boldsymbol{X}}{\mathrm{D}t} = \frac{\partial\varphi}{\partial s}\boldsymbol{s} + \frac{\partial\varphi}{\partial n}\boldsymbol{n}, \tag{7.2}$$

where D is used to indicate a material derivative, $\varphi(\boldsymbol{X})$ is the potential of a fluid particle on the free surface at the location $\boldsymbol{X}$. The vectors $\boldsymbol{s}$ and $\boldsymbol{n}$ are respectively tangent and normal to the free surface. A Neumann boundary condition is imposed on the hull as a result of the body boundary condition (2.7) as well as on the axes of symmetry below the hull. Far from the ship, the inner fluid domain is bounded by a circular control surface (see figure 1) on which is applied a Robin–Fourier condition:

$$\varphi + r\frac{\partial\varphi}{\partial n} = 0, \tag{7.3}$$

in order to enforce the matching condition (3.11) between the bow flow and far-field flow solutions. At each time step, this set of boundary conditions allows the potential and its normal derivative to be computed through the resolution of the integral equation:

$$\theta(M)\varphi(M) = \int_{\Sigma}\left[\varphi(P)\frac{\partial G}{\partial n_p}(M,P) - \frac{\partial\varphi}{\partial n_p}(P)\,G(M,P)\right]\mathrm{d}s_p, \tag{7.4}$$

where M is a point on the boundary, G is the simple source Green function, $\theta(M)$ is the included angle, or the angle between two tangents of the boundary (equal to π for a smooth curve) and s is a curvilinear abscissa along the boundary Σ. Equation (7.4) is discretized using a standard collocation method. The boundary of the computational domain is approximed by segments and φ and φ_n are assumed to vary linearly along each segment. The numerical procedure is then reduced to the integration of equations (7.1) and (7.2) starting from initial conditions for the free-surface elevation and the associated potential.

Ideally, the initial condition should be given by (5.4) but it was found that using these initial conditions directly tends to generate the so-called sawtooth instability that renders the nonlinear simulation unstable as the grid space goes to zero. Instead of classically controlling the growth of these instabilities by smoothing the solution, we suppressed them by using initial conditions derived from the analytical solution for a thin ship. Under this assumption, the results by Peregrine (1972) and Roberts (1987) for the transient free-surface flow generated by a moving vertical plate can be used to describe the bow flow along a thin wall-sided hull. The short-time expansion of the solution was used for the free-surface elevation, and the potential on the free surface was taken as the integral in time of the surface displacement, according to the linear dynamic free-surface condition. The numerical program has been verified by comparing with the analytical results for a thin wedge-shaped bow. It was found that the nonlinear numerical solution converges (within graphical accuracy) to the linear analytical solution as the apex angle α goes to zero. It has also been checked that Ogilvie's (1972) and Roberts's (1987) results agree for the wave profile along the hull. For the case of a non-vertical wall-sided hull, following Maruo & Song (1994), the self-similar solution corresponding to the two-dimensional wedge entry problem with small apex angle (Cointe 1991) was used to start the computation instead.

7.3. *Composite solution*

The composite solution is constructed by adding the near-bow solution to the bow one and subtracting the common part of the two developments. For the case of a thin ship, the common part is given by (5.3). This expression can be interpreted as the solution of the two-dimensional Laplace equation subject to the body boundary condition on the exact location of the hull and an homogeneous Dirichlet condition for the potential on the undisturbed free surface. In the case of a slender ship, the common part is computed in a similar way to the bow flow solution, i.e. using the MEL method, except that the free-surface conditions are modified accordingly. The correction to be added to the nonlinear bow solution is equal to the difference between the near-bow solution and the common part. Since the correction is small and is obtained from the difference between two large quantities, it was found necessary to avoid interpolation errors between the different meshes. The near-bow solution for the free-surface elevation is therefore evaluated at the same points as the common part. Even so, smoothing had to be introduced to get rid of the oscillations that arise for large values of x/h, as the value of the correction goes to zero.

8. Validation

8.1. *Gravity-free flow*

According to the present theory, the wave elevation in front of the bow does not depend on the speed of the ship. This property results from the fact that gravity effects can be neglected to first order in the near-bow domain and therefore also in the general case. In the case of a thin vertical-sided hull, the wave elevation does not depend on the precise shape of the hull, but only on the draught h and the apex angle α. The wave elevation at the edge of the bow can be obtained by taking the limit of (6.2) as $\hat{x} \to 0$ and $\hat{y} \to 0$, leading to

$$\eta(0,0) = \frac{\tan\alpha\, h}{\pi}. \tag{8.1}$$

In this last expression, $\tan\alpha$ is assumed to be small. This result differs from the result of Sclavounos (1994) who predicted half the value of (8.1) using a different approach. The fact that the three independent solutions in the bow, near-bow and far-field domains match indicates that (8.1) is the correct theoretical value. This result has been compared with experiments presented by Fontaine & Cointe (1997). However, the effect of surface tension is important in these experiments because of the small size of the model tested. The results can nevertheless be scaled to full scale by introducing a surface tension parameter $F_h\sqrt{\sigma/(\rho g)}/h$, where $\sigma \simeq 72.8 \times 10^{-3}\,\mathrm{N\,m^{-1}}$, so that full scale corresponds to that surface tension parameter going to zero (see Fontaine & Faltinsen 1997). The results then show that (8.1) is reasonable. This is also confirmed by the experiments performed at a larger scale by Larrarte (1994) in the towing tank of Ecole Centrale de Nantes (60 m length, 5 m width, 2.5 m depth). The flat-bottom wall-sided hull has an identical parabolic shape at the bow and the stern, while the centre part of the ship consists of a simple rectangular cylinder of one third the total length of the ship. The apex angle at the bow is $\alpha = 20^\circ$, the draught is $h = 0.2$ m and the total length of the model is 1.5 m. Results for the wave profile along the hull are presented in figure 6. The lowest F_h values do not show the character of a high-Froude-number flow at the bow; in particular the free-surface elevation has already reached its maximum at the nose. For the higher values ($F_h = 0.664$ and larger), the

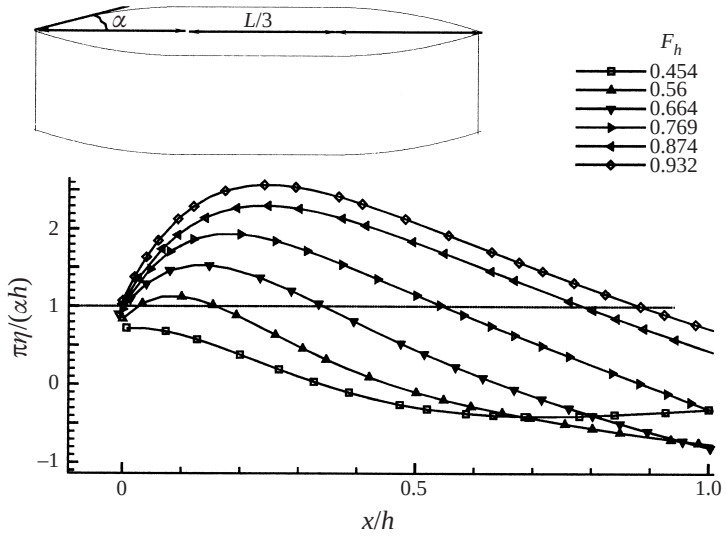

FIGURE 6. Wave profile along a wall-sided parabolic bow with apex angle $\alpha = 20°$ and draught $h = 0.2$ m. Experiments were performed by Larrarte (1994) at Ecole Centrale de Nantes.

difference between (8.1) and the experiment is less than 10% although the perturbation parameter is not small ($\tan\alpha \simeq 0.36$). One may therefore hope that a higher-order solution in terms of α may explain this small difference. The near-bow flow solution (6.2) is singular at the apex of the wedge since the slope of the free surface tends to infinity. This suggests that strong vertical gradients arise near the contact point.

Very close to the bow, Dong *et al.* (1997) observed that a very thin and instable liquid sheet develops on the body. In the following discussion, we interpret some of their experimental results in the light of our theoretical approach. Their measurements show that the vertical velocity near the body gradually decreases as the depth increases, and changes sign at a given depth which would seem to be independent of the Froude number (see their figures 8 and 13). From a theoretical point of view, the bow flow solution can be described by the small-time expansion by Peregrine (1972) or Roberts (1987) close to the nose. This solution is however singular at the intersection between the body and the free surface because of its high oscillatory behaviour. The singularity can be removed by considering the effects of surface tension (Joo, Schultz & Messiter 1990), so that the resulting solution is regular and does not depend on gravity. This implies that the overall flow close to the nose is not affected by gravity, which is in agreement with the observations by Dong *et al.* (1997) that the length scale describing the flow close to the nose does not depend on the Froude number. Figure 7 shows the composite solution for the velocity field and wave elevation in the case of a parabolic wall-sided bow. As observed, the vertical velocity changes its sign on the hull. The liquid below moves towards the bottom of the ship and the liquid above is (or more precisely will be) involved in the wave motion. Further away from the body, the upward trend extends to a larger depth as a result of the dipole-like behaviour of the asymptotic solution.

8.2. *Diverging waves*

The linear solution for the flow around a thin bow (Roberts 1987) involves the length scales hF_h in the longitudinal direction and h in the transverse ones. For values of the Froude number F_h larger than 1, this scaling is confirmed by the experimental

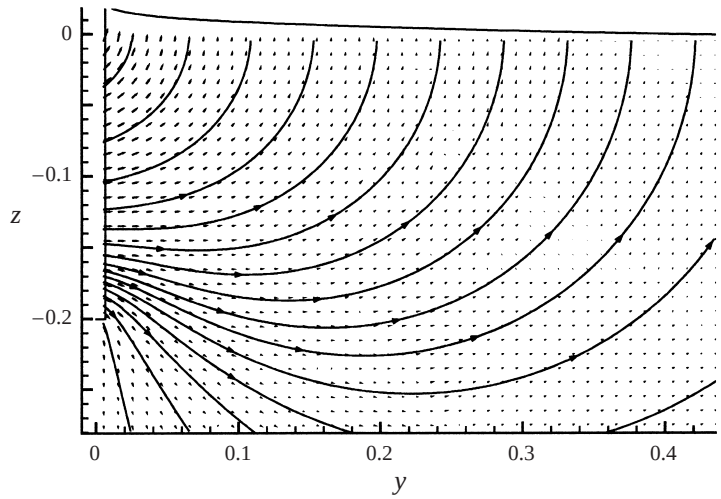

FIGURE 7. Linear composite solution for the flow around a wedge-shaped bow, $\alpha = 20°$, $h = 0.2\,\mathrm{m}$, $F_h = 0.93$ in the cross-section $x = 0.025\,\mathrm{m}$.

results by Ogilvie (1972), Calisal & Chan (1989) and Miyata & Inui (1984) in the case of a wedge-shaped bow. Figure 8 shows a comparison between numerical and experimental results by Larrarte (1994) for the wave profile along the hull. The Froude number F_h is equal to 0.93 and the perturbation parameters δ and α are respectively 0.13 and 0.35 so that this case clearly appears as a limiting one from an asymptotic point of view. The simulation leads to a fairly good prediction of the bow wave height, but the longitudinal position at which the maximum occurs is over-estimated. In the present case, measurements show that the perturbation of the flow in the longitudinal direction is not completely negligible in comparison to that in the transverse direction (Miyata & Inui 1984). Similar trends were obtained by Calisal & Chan (1989) for a wedge-shaped bow, and by Faltinsen (1983) on realistic ships, including both a Series 60 hull, $C_b = 0.6$ at Froude numbers $F_L = 0.22$, 0.28 and 0.35, and a Wigley hull at $F_L = 0.266$. In this last case, the longitudinal position of the maximum is correctly predicted at $F_L = 0.348$ and 0.452. At higher Froude numbers, Faltinsen & Zhao (1991*b*) and Fontaine & Cordier (1997) also reported good agreement for the wave profile along the hull of a high-speed ship.

An example of a high-resolution nonlinear computation for the wave field around a Wigley hull at Froude number $F_L = 0.5$ is presented in figure 9. The numerical simulation was achieved using 35 points per draught, leading to the equivalent of 10^6 points on the free surface. The simulation was performed over twice the length of the ship in order to illustrate the global pattern of the flow. Very close to the bow, the free surface rises rapidly leading eventually to the formation of a jet. This splash would seem to be an impact-like phenomenon as discussed earlier. The rising water is then halted by the action of gravity and falls, in the process creating a strong diverging wave crest (A) which radiates out away from the body. This may then be followed by one or more divergent crests, (B) in the present case, probably due to dispersive effects. Behind the ship, a 'rooster tail' is formed, which also would seem to create diverging waves in the wake as the result of its release, in a Poisson-like problem. For a transom stern, it is likely that a near stern solution should be introduced.

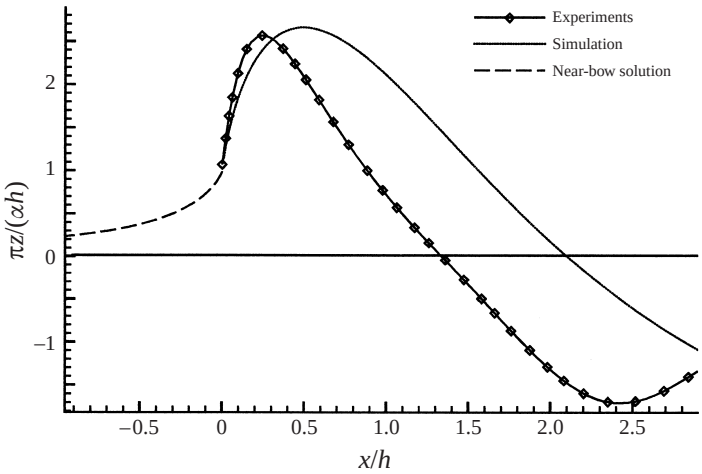

FIGURE 8. Wave profile along a wall-sided parabolic hull with apex angle $\alpha = 20^\circ$ and draught $h = 0.2\,\mathrm{m}$ at $F_h = 0.93$. The discrepancy between the experiment and the simulation results from the large value of $\tan\alpha \simeq 0.35$, clearly not small compared to unity. Experiments were performed by F. Larrarte (1994) at Ecole Centrale de Nantes.

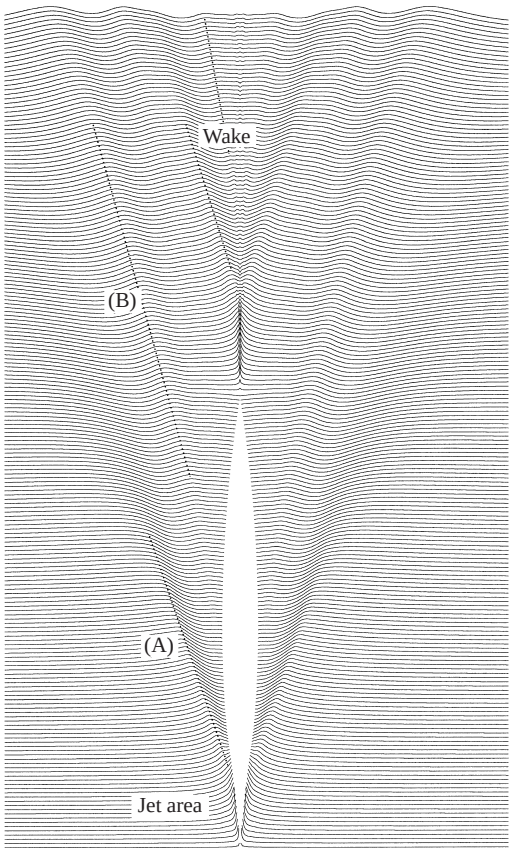

FIGURE 9. Diverging waves generated by a Wigley hull, $F_L = 0.5$, $h/L = 0.1$ and $b/L = 0.075$.

Since the simplified approach does not include the transverse wave system, it should be used where the diverging wave system is dominating. In the case of high-speed ships, the transverse waves eventually become longer enough that they appear only in the wake of the ship, thus justifying the use of the present approach over the whole ship length. This is confirmed by the successful comparisons between the wave fields obtained with both the present theory and three-dimensional thin-ship linear computations (Faltinsen & Zhao 1991*b*). Even for a slower ship, the diverging wave pattern obtained matches in great detail the features calculated by solving the three-dimensional nonlinear boundary value problem (Tulin & Wu 1996).

As the Froude number increases, the angle between the bow wave and the model axis decreases. The point along the body at which the wave detaches from the model moves further downstream. The distance between the waves increases and the wave crest become straighter (less curved). These trends are consistent with the observations reported by Dong *et al.* (1997) and Miyata & Inui (1984) although variations of the wave angle could appear in contrast to prediction by classical three-dimensional linear theory that the wave field is contained within the constant Kelvin angle. This pattern is however observed very far from the ship and is not described within the present analysis which focuses attention on the flow in the vicinity of the ship. From a theoretical point of view, the asymptotic study presented here could certainly be completed by including a far-field analysis similar to the one performed by Cole (1988) in the case of high-speed planing ships. Using the length scale U^2/g, the high-speed ship appears as a pressure disturbance moving on the free surface, and the corresponding linear solution predicts three-dimensional features such as the Kelvin angle.

9. Conclusions

The steady free-surface potential flow around a slender or thin hull has been studied. It has been demonstrated that the method of matched asymptotic expansions provides a consistent perturbation procedure for the justification of a 'parabolic' approximation of the equations. Due to the slenderness assumption, the flow in the vicinity of the hull is two-dimensional in each cross-section. However, three-dimensional effects are important in front of the bow and yield a correction to the two-dimensional solution. This correction arises through the composite solution. The asymptotic analysis is then used to explain the structure of the bow wave in connection with experimental results. The mixed Eulerian Lagrangian method is then applied to solve the nonlinear near-field flow and numerical results are presented. Since the MEL method allows the overturning phase of breaking to be simulated, at least until the jet re-enters the front face of the wave, the nonlinear high-speed slender body theory presented here appears as an interesting alternative to the resolution of the three-dimensional nonlinear problem for both, bow breaking waves and the entire flow around a high-speed ship.

E.F. is grateful to all the people that have made this study possible, in particular F. Desit and S. Cordier, to the French Navy and Bassin d'Essais des Carènes for the financial support, G. Delhommeau and F. Larrarte from Ecole Centrale of Nantes where experimental studies were performed, and finally M. P. Tulin and T. Lamont-Smith from the University of California at Santa Barbara, Ocean Engineering Laboratory, respectively for their fruitful discussions and patient proof-reading of this manuscript.

Appendix A. Near-bow flow solution

In this Appendix, we demonstrate that the near-bow flow solution for a thin ship given by (4.14) satisfies the simplified body boundary condition (4.7). From (4.14), it follows that

$$2\pi \lim_{\hat{y}\to 0^+} \frac{\partial \breve{\varphi}_1}{\partial \hat{y}} = \lim_{\hat{y}\to 0^+} \int_{-1}^{0} G^-(\hat{x},\hat{y},\hat{z},s)\, f_{\breve{x}}(0,s)\,\mathrm{d}s - \lim_{\hat{y}\to 0^+} \int_{-1}^{0} G^+(\hat{x},\hat{y},\hat{z},s)\, f_{\breve{x}}(0,s)\,\mathrm{d}s, \tag{A 1}$$

where

$$G^-(\hat{x},\hat{y},\hat{z},s) = \frac{1}{-\hat{x}+\left(\hat{x}^2+\hat{y}^2+(\hat{z}-s)^2\right)^{1/2}} \frac{\hat{y}}{\left(\hat{x}^2+\hat{y}^2+(\hat{z}-s)^2\right)^{1/2}}, \tag{A 2}$$

$$G^+(\hat{x},\hat{y},\hat{z},s) = \frac{1}{-\hat{x}+\left(\hat{x}^2+\hat{y}^2+(\hat{z}+s)^2\right)^{1/2}} \frac{\hat{y}}{\left(\hat{x}^2+\hat{y}^2+(\hat{z}+s)^2\right)^{1/2}}. \tag{A 3}$$

Since $f_{\breve{x}}(0,s)$ is regular for $s\in[-1,0]$, and $\lim G^+ = 0$ as $\hat{y}\to 0^+$ for $\hat{z}\in[-1,0]$ and for all $s\in[-1,0]$, it follows that the second term of the right-hand side of (A 1) is equal to zero. The first term can be written as

$$\lim_{\hat{y}\to 0^+} \int_{-1}^{0} G^-(\hat{x},\hat{y},\hat{z},s)\, f_{\breve{x}}(0,s)\,\mathrm{d}s = \lim_{\hat{y}\to 0^+} \left[\int_{-1}^{\hat{z}-\epsilon} + \int_{\hat{z}-\epsilon}^{\hat{z}+\epsilon} + \int_{\hat{z}+\epsilon}^{0} G^-(\hat{x},\hat{y},\hat{z},s)\, f_{\breve{x}}(0,s)\,\mathrm{d}s\right]$$
$$= \lim_{\hat{y}\to 0^+} \int_{\hat{z}-\epsilon}^{\hat{z}+\epsilon} G^-(\hat{x},\hat{y},\hat{z},s)\, f_{\breve{x}}(0,s)\,\mathrm{d}s, \tag{A 4}$$

where ϵ is a small positive number. Using the previous arguments leads to the conclusion that the only contribution comes from the singularity for $y=0$ and $s=\hat{z}$. This contribution is evaluated using a Taylor expansion:

$$\lim_{\hat{y}\to 0^+} \int_{\hat{z}-\epsilon}^{\hat{z}+\epsilon} G^-(\hat{x},\hat{y},\hat{z},s)\, f_{\breve{x}}(0,s)\,\mathrm{d}s = \lim_{\hat{y}\to 0^+} \int_{\hat{z}-\epsilon}^{\hat{z}+\epsilon} \frac{f(0,\hat{z})}{-\hat{x}+\hat{x}\left[1+\frac{1}{2}\left(\frac{\hat{y}}{\hat{x}}\right)^2+\frac{1}{2}\left(\frac{\hat{z}-s}{\hat{x}}\right)^2\right]} \times \frac{\hat{y}}{\hat{x}\left[1+\frac{1}{2}\left(\frac{\hat{y}}{\hat{x}}\right)^2+\frac{1}{2}\left(\frac{\hat{z}-s}{\hat{x}}\right)^2\right]} [1+o(1)]\,\mathrm{d}s$$
$$= \lim_{\hat{y}\to 0^+} \int_{\hat{z}-\epsilon}^{\hat{z}+\epsilon} \frac{2\hat{y}}{\hat{y}^2+(\hat{z}-s)^2} f_{\breve{x}}(0,\hat{z})\,\mathrm{d}s$$
$$= 4 f_{\breve{x}}(0,\hat{z}) \lim_{\hat{y}\to 0^+} \arctan(\epsilon/\hat{y})$$
$$= 2\pi\, f_{\breve{x}}(0,\hat{z}). \tag{A 5}$$

As a result, the body boundary condition (4.7) is satisfied.

Appendix B. Asymptotic behaviour of the different solutions

In the limit processes described above, it is understood that $\delta \ll \xi(\delta) \ll 1$ and $r_\xi = O(1)$, $x_\xi = O(1)$:

$$\lim_{\substack{\delta\to 0\\ r_\chi = O(1)}} \delta\breve{\varphi}_1\left(\hat{x}, \frac{\chi(\delta)}{\delta} r_\chi, \theta\right)$$

$$= \frac{\delta}{2\pi}\int_{-1}^{0} f_{\bar{x}}(0,\zeta)\ln\left[\frac{-\dfrac{\chi(\delta)}{\delta}x_\chi + \left(\hat{x}^2 + \left(\dfrac{\chi(\delta)}{\delta}r_\chi\cos\theta\right)^2 + \left(\dfrac{\chi(\delta)}{\delta}r_\chi\sin\theta - \zeta\right)^2\right)^{1/2}}{-\dfrac{\chi(\delta)}{\delta}x_\chi + \left(\hat{x}^2 + \left(\dfrac{\chi(\delta)}{\delta}r_\chi\cos\theta\right)^2 + \left(\dfrac{\chi(\delta)}{\delta}r_\chi\sin\theta + \zeta\right)^2\right)^{1/2}}\right]\mathrm{d}\zeta$$

$$= \frac{\delta}{2\pi}\int_{-1}^{0} f_{\bar{x}}(0,\zeta)\left[\frac{-2\sin\theta}{\dfrac{\chi(\delta)}{\delta}r_\chi}\zeta + O\left[\left(\frac{\delta}{\chi(\delta)}\right)^2\right]\right]\mathrm{d}\zeta$$

$$= -\frac{\delta^2}{\chi(\delta)}\frac{\sin\theta}{r_\chi}\frac{1}{\pi}\int_{-1}^{0}\zeta\, f_{\bar{x}}(0,\zeta)\,\mathrm{d}\zeta + O\left[\frac{\delta^3}{\chi(\delta)^2}\right]; \tag{B 1}$$

$$\lim_{\substack{\delta\to 0\\ r_\chi = O(1)}} \delta^2\tilde{\varphi}_1(\delta\hat{x}, \chi(\delta)r_\chi, \theta) = -\frac{\delta^2\sin\theta}{4\pi\tilde{r}}\int_{-\tilde{x}/\tilde{r}}^{\infty}\frac{\mu(\tilde{r}s'' + \tilde{x})}{(s''^2+1)^{3/2}}\,\mathrm{d}s'' \quad \text{with} \quad s'' = \frac{s-\tilde{x}}{\tilde{r}}$$

$$= -\frac{\sin\theta}{4\pi r_\chi}\frac{\delta^2}{\chi(\delta)}\int_{-\frac{\delta}{\chi(\delta)}\frac{\hat{x}}{r_\chi}}^{\infty}\frac{\mu(\chi(\delta)r_\chi s'' + \delta\hat{x})}{(s''^2+1)^{3/2}}\,\mathrm{d}s''$$

$$= -\mu(0)\frac{\sin\theta}{4\pi r_\chi}\frac{\delta^2}{\chi(\delta)}\int_0^{\infty}\frac{1}{(s''^2+1)^{3/2}}(1+o(1))\,\mathrm{d}s''$$

$$= -\frac{\delta^2}{\chi(\delta)}\frac{\sin\theta}{r_\chi}\frac{\mu(0)}{4\pi} + o\left[\frac{\delta^2}{\chi(\delta)}\right]; \tag{B 2}$$

$$\lim_{\substack{\delta\to 0\\ x_\chi = O(1)\\ x_\chi < 0}} \delta\breve{\varphi}_1\left(\frac{\chi(\delta)}{\delta}x_\chi, \hat{r}, \theta\right)$$

$$= \frac{\delta}{2\pi}\int_{-1}^{0} f_{\bar{x}}(0,\zeta)\,\ln\left[\frac{-\dfrac{\chi(\delta)}{\delta}x_\chi + \left(\left(\dfrac{\chi(\delta)}{\delta}x_\chi\right)^2 + \hat{y}^2 + (\hat{z}-\zeta)^2\right)^{1/2}}{-\dfrac{\chi(\delta)}{\delta}x_\chi + \left(\left(\dfrac{\chi(\delta)}{\delta}x_\chi\right)^2 + \hat{y}^2 + (\hat{z}+\zeta)^2\right)^{1/2}}\right]\mathrm{d}\zeta$$

$$= \frac{\delta}{2\pi}\int_{-1}^{0} f_{\bar{x}}(0,\zeta)\left[-\frac{\hat{r}\sin\theta}{\left(\dfrac{\chi(\delta)}{\delta}x_\chi\right)^2}\zeta + O\left[\left(\frac{\delta}{\chi(\delta)}\right)^4\right]\right]\mathrm{d}\zeta$$

$$= -\frac{1}{2\pi}\frac{\delta^3}{\chi(\delta)^2}\frac{\hat{r}\sin\theta}{{x_\chi}^2}\int_{-1}^{0}\zeta\, f_{\bar{x}}(0,\zeta)\,\mathrm{d}\zeta + o\left[\frac{\delta^3}{\chi(\delta)^2}\right]; \tag{B 3}$$

$$\lim_{\substack{\delta\to 0\\ x_\chi = O(1)\\ x_\chi<0}} \delta^2\,\tilde{\varphi}_1(\chi(\delta)x_\chi, \delta\hat{r}, \theta)$$

$$= \delta^2 \int_0^\infty \frac{-\mu(s)}{4\pi} \frac{\delta\hat{r}\,\sin(\theta)}{\left[(\chi(\delta)x_\chi - s)^2 + (\delta\hat{r})^2\right]^{3/2}}\,\mathrm{d}s$$

$$= -\frac{1}{4\pi}\frac{\delta^3}{\chi(\delta)^2}\,\hat{r}\sin\theta \int_0^\infty \frac{\mu(\chi(\delta)s')}{\left[(x_\chi - s')^2 + \left(\frac{\delta}{\chi(\delta)}\hat{r}\right)^2\right]^{3/2}}\,\mathrm{d}s' \quad \text{with} \quad s' = \frac{s}{\chi(\delta)}$$

$$= -\frac{1}{4\pi}\frac{\delta^3}{\chi(\delta)^2}\,\hat{r}\sin\theta \int_0^\infty \frac{1}{(x_\chi - s')^3} \frac{\mu(\chi(\delta)s')}{\left[1 + \left(\frac{\delta\hat{r}}{\chi(\delta)(x_\chi - s')}\right)^2\right]^{3/2}}\,\mathrm{d}s'$$

$$= -\frac{1}{4\pi}\frac{\delta^3}{\chi(\delta)^2}\,\hat{r}\sin\theta \int_0^\infty \frac{1}{(x_\chi - s')^3}\,[\mu(0) + O(\chi(\delta))]\left[1 + O\left(\frac{\delta}{\chi(\delta)}\right)\right]\mathrm{d}s'$$

$$= -\frac{\mu(0)}{4\pi}\frac{\delta^3}{\chi(\delta)^2}\hat{r}\sin\theta \int_0^\infty \frac{1}{(x_\chi - s')^3}\,\mathrm{d}s' + o\left[\frac{\delta^3}{\chi(\delta)^2}\right]$$

$$= -\frac{\delta^3}{\chi(\delta)^2}\frac{\mu(0)}{8\pi}\frac{\hat{r}\sin\theta}{x_\chi^2} + o\left[\frac{\delta^3}{\chi(\delta)^2}\right]$$

$$= -\delta\,\frac{\mu(0)}{8\pi}\frac{\hat{r}\sin\theta}{\hat{x}^2} + o(\delta). \tag{B 4}$$

REFERENCES

Calisal, S. M. & Chan, J. L. K. 1989. A numerical modeling of ship bow waves. *J. Ship Res.* **33**, 21–28.

Chapman, R. B. 1975 Numerical solution for hydrodynamics forces on a surface piercing plate oscillating in yaw and sway. In *Proc. 1st Intl Conf. Numer. Ship Hydrodyn., Gaithersberg, MD*, pp. 333–350. Naval Ship Research and Development Center, Bethesda.

Chapman, R. B. 1976 Free surface effects for yawed surface-piercing plate. *J. Ship Res.* **20**, 125–136.

Cointe, R. 1989 Two-dimensional water-solid impact. *J. Offshore Mech. Artic Engng* **111**, 237–243.

Cointe, R. 1990 Numerical simulation of a wavetank. *Engng Anal. with Boundary Elements* **7**, 167–177.

Cointe, R. 1991 Free-surface flows close to a surface piercing body. In *Mathematical Approaches in Hydrodynamics* (ed. T. Miloh), pp. 319–334. SIAM.

Cole, S. 1988 A simple example from flat-ship theory. *J. Fluid Mech.* **189**, 301–310.

Delhommeau, G. 1987 Les problèmes de diffraction-radiation et de résistance de vagues: étude théorique et résolution numérique par la méthode des singularités. Thèse de Doctorat d'Etat, ENSM de Nantes, Laboratoire d'Hydrodynamique Navale.

Dong, R. R., Katz, J. & Huang, T. T. 1997 On the structure of bow waves on a ship model. *J. Fluid Mech.* **346**, 77–115.

Faltinsen, O. M. 1977 Numerical solutions of transient nonlinear free surface motion outside and inside moving bodies. In *Proc. Second Intl Conf. on Numerical Ship Hydrodynamics, Berkeley, California*, pp. 347–357.

Faltinsen, O. M. 1983 Bow flow and added resistance of slender ships at high Froude number and low wave lengths. *J. Ship Res.* **27**, 160–171.

Faltinsen, O. M. 1993 On seakeeping of conventional and high-speed vessels. *J. Ship Res.* **37**, 87–101.

Faltinsen, O. M. & Zhao, R. 1991*a* Numerical prediction of ship motions at high forward speed. *Phil. Trans. R. Soc. Lond.* A **334**, 241–252.

Faltinsen, O. M. & Zhao, R. 1991*b* Flow prediction around high-speed ships in waves. In *Mathematical Approaches in Hydrodynamics* (ed. T. Miloh), pp. 265–288. SIAM.

Fontaine, E. 1996 Simulation de l'écoulement potentiel engendré par un corps élancé perçant la surface libre à forts nombres de Froude. Thèse de Doctorat de l'Ecole Nationale des Ponts et Chaussées, Paris.

Fontaine, E. & Cointe, R. 1997 A Slender Body Approach to Nonlinear Bow Waves. *Phil. Trans. R. Soc. Lond.* A **355**, 565–574.

Fontaine, E. & Cordier, S. 1997 Recent Experience using high-speed slender body theory. In *Proc. 4th Intl Conf. on Fast Sea Transportation, Sydney*, vol. 1, pp. 405–411. Baird Publications.

Fontaine, E. & Faltinsen, O. M. 1997 Steady flow near a wedge shaped bow. In *Proc. 12th Intl Workshop on Water Waves and Floating Bodies, Marseille* (ed. B. Molin), pp. 75–79.

Fontaine, E. & Tulin, M. P. 1998 On the prediction of nonlinear free-surface flows past slender hulls using $2D + t$ theory: the evolution of an idea. In *Proc. RTO/AVT Symp. on Fluid Dynamics Problems of Vehicles Operating near or in the Air-sea Interface, Amsterdam.* RTO MP-15, pp. 26-1–26-10.

Fritts, M. J., Meinhold, M. J. & Von Kerczek, C. H. 1988 The calculation of nonlinear bow waves. *Proc. 17th ONR Symp. on Naval Hydrodynamics*, pp. 485–498.

Joo, S. W., Schultz, W. W. & Messiter, A. F. 1990 An analysis of the initial-value wavemaker problem. *J. Fluid Mech.* **214**, 161–183.

Kàrmàn, Th. von 1929 The impact on seaplane floats during landing. *NACA* 321.

Kevorkian, J. & Cole, J. D. 1981 *Perturbation Method in Applied Mathematics.* Springer.

Larrarte, F. 1994 Etude expérimentale et théorique des profils de vagues le long d'une carène. Thèse de Doctorat de l'Ecole Centrale de Nantes.

Longuet-Higgins, M. S. & Cokelet, E. D. 1976 The Deformation of Steep Surface Waves on Water, I. A Numerical Method of Computation. *Proc. R. Soc. Lond.* A **350**, 1–26.

Maruo, H. & Song, W. 1994 Nonlinear analysis of bow wave breaking and deck wetness of a high-speed ship by the parabolic approximation. In *20th Symp. on Naval Hydrodynamics, University of California, Santa Barbara*, pp. 68–82. National Academy Press, Washington, DC.

Mitchell, P. 1898 The wave resistance of a ship. *Phil. Mag.* (5) **45**, 106–124.

Miyata, H. & Inui, T. 1984 Nonlinear ship waves. *Adv. Appl. Mech.* **24**, 215–289.

Ogilvie, T. F. 1972 The wave generated by a fine ship bow. In *Ninth Symp. Naval Hydrodynamics, Paris* (ed. R. Brard & A. Castaro), vol. 2, pp. 1483–1525. National Academy Press, Washington, DC.

Ogilvie, T. F. 1967 Nonlinear high-Froude-number free-surface problems. *J. Engng Maths* **1**, 215–235.

Peregrine, D. H. 1972 *Unpublished notes.*

Roberts, A. J. 1987 Transient free-surface flows generated by a moving vertical plate. *Q. J. Mech. Appl. Maths* **40**, 129.

Sclavounos, P. 1994 On the intersection near a fine ship bow. In *Twentieth Symp. on Naval Hydrodynamics, University of California, Santa Barbara*, pp. 934–945. National Academy Press, Washington, DC.

Tulin, M. P. 1957 The theory of slender surfaces planing at high speed. *Schiffstechnik* **4**, 125–133.

Tulin, M. P. & Wu, M. 1996 Divergent Bow Waves. In *Twenty First Symp. on Naval Hydrodynamics, Trondheim, Norway*, pp. 99–117. National Academy Press, Washington, DC.

Wagner, H. 1932 Über Stoβ und Gleitvorgänge an der Oberfläche von Flüssigkeiten. *Z. Angew. Math. Mech.* **12**, 193–215.

Ward, G. N. 1955 *Linearized Theory of Steady High-Speed Flow.* Cambridge University Press.

Wu, M., Fontaine, E. & Tulin, M. P. 2000 Deck-wetness and slamming modeling. To appear in *J. Ship Res.*

Zhao, R. & Faltinsen, O. M. 1999 A nonlinear method for predicting wave resistance of ships. In *Proc. 14th Intl Workshop on Water Waves and Floating Bodies, Port Huron, Michigan* (ed. R. Beck), pp. 175–179.